Polymers **2014**, *6*, 2803-2818; doi:10.3390/polym6112803

OPEN ACCESS

polymers

ISSN 2073-4360

www.mdpi.com/journal/polymers

Review

Stimuli-Responsive Polymers and Colloids under Electric and Magnetic Fields

Wen Ling Zhang † and Hyoung Jin Choi †,*

Department of Polymer Science and Engineering, Inha University, Incheon 402-751, Korea;
E-Mail: wenling86@naver.com

† These authors contributed equally to this work.

* Author to whom correspondence should be addressed; E-Mail: hjchoi@inha.ac.kr;
Tel./Fax: +82-32-865-5178.

External Editor: Michael K. C. Tam

Received: 15 July 2014; in revised form: 20 October 2014 / Accepted: 30 October 2014 / Published: 5 November 2014

Abstract: Electrorheological (ER) and magnetorheological (MR) suspensions undergo a reverse phase transition from a liquid-like to solid-like state in response to an external electric or magnetic field, respectively. This paper briefly reviews various types of electro- or magneto-responsive materials from either polymeric or inorganic and hybrid composite materials. The fabrication strategies for ER/MR candidates and their ER/MR characteristics (particularly for ER fluids) are also included.

Keywords: electrorheological; magnetorheological; suspension; phase transition

---

1. Introduction

Extensive smart functional materials that can respond to external stimuli, such as temperature, mechanical stress, pH, and electric or magnetic fields, have recently become hot topics in both academia and industry [1–5]. Among these, electric and magnetic stimuli-responsive systems have attracted considerable attention because of their easy controllability and industrial needs. Suspensions containing electro-responsive and magneto-responsive particles are often referred to as electrorheological (ER) or magnetorheological (MR) fluids [6–25], respectively, in which the ER fluid generally consists

of dielectric polarizable particles dispersed in an insulating medium, whereas its magnetic analogue, the MR fluid, is typically based on magnetizable particles dispersed in a carrier medium. When exposed to an electric field, the suspended ER particles become electrically polarized, resulting in the formation of a fibrous structure of originally uniformly distributed particles. Similarly, the MR particles generate a dipole moment to form chain/column aggregates under an external magnetic field. The field-induced structures restrict the free flow of dispersed particles in ER/MR suspensions, thereby inducing significant variations in their rheological and viscoelastic properties including yield stress, flow curve, enhanced apparent viscosity, creep, recovery, and dynamic moduli [26,27]. The interesting smart electro/magneto-responsive characteristics of fine tuning and the quick response make them appropriate candidates in broad engineering areas, such as clutches, seismic vibration dampers, breaks, optical finishing systems, medical therapies, artificial muscle stimulators, actuators, haptic master, micro-fluidic control, and viscosity reduction of crude oil [24,28–35]. Nevertheless, compared to conventional ER fluids, MR suspensions generally exhibit a higher field-induced effect and are in less demand by electric providers.

In addition, various factors are known to affect ER and MR characteristics. In the case of ER fluids, their effects can be influenced by temperature, electric field strength, particle concentration, particle size, dispersed particle geometry, *etc.* Wang *et al*. [36] reported that particles with smaller size and good wettability are favorable to their ER characteristics. Interestingly, the mixture of micro-spherical particles (50:50) exhibited highest ER effects compared to the pure small and large monodisperse particles [37]. The optimum ER properties can be observed at a relatively higher temperature and relatively higher particle concentration [38]. El Wahed [39] has showed the results that the highest effectiveness of the capacity of the transmitted force in the ER fluid based short-stroke damper is obtained at high solid particle faction.

While many review papers separately covering either ER or MR fluids are available, it has been seldom reviewed together. In this short review paper, focus is being given to the strategies of fabrication for ER and MR materials together in the viewpoint of polymers and colloids, their interesting morphology and an analysis of their rheological properties.

2. Materials

The typical dispersed phase of ER fluids is composed of polarizable colloidal particles with a size range of 0.1–100 μm, which is favorable for improving the ER effect, because particles too small cause Brownian motion and particles too large have sedimentation problems. Diverse polarizable particles, such as corn starch, cellulose, aluminosilicate, TiO_2, and SiO_2 gels can be classified as hydrous ER systems, in which the existence of moisture adsorbed on the surface of the particles plays a critical role in their ER effect. On the other hand, the presence of water in wet-base aqueous ER systems restricts their engineering applications with a narrow operating temperature range and potential corrosion of the device. Therefore, anhydrous ER systems with enhanced stability have been applied extensively to discovering promising applications for the ER fluids, including carbonaceous materials, semiconducting polymers, such as polyaniline (PANI), polypyrrole (PPy), poly(*p*-phenylene) (PPP), and poly(phenylenediamine), dehydrated zeolites, and other dielectric inorganics [40–43].

As for their ER mechanism, Clercx and Bossis [44] reported the electrostatic interactions of spheres using a multipole-expansion theory, which is favorable for understanding the electrostatic forces between ER particles and monitoring their ER properties effectively. The interaction and energy balance of field-controllable electric and magnetic dipoles was also investigated [45,46]. On the other hand, a chain model was developed to analyze the ER fluid in both steady and oscillatory shear, concentrating on the mechanical stability of the electric field-induced chains [47]. Martin *et al*. [48] have also studied the structure and dynamics of ER fluids in quiescent state and under steady and oscillatory shear using a light scattering [48]. Espin *et al*. have studied ER effects of iron (III) oxide based ER fluid with different particle concentration under various electric fields, Mason number, M_n was introduced to describe the relationship of relative viscosity and shear rate at a constant volume fraction [49]. Hybrid composites of these materials with different morphologies are known to play an important role in their ER effects and will be discussed briefly in the following next section.

Concurrently, in MR fluids, magnetic particles, such as iron, iron oxides (Fe_2O_3 and Fe_3O_4), and carbonyl iron (CI), have been developed owing to their high saturation magnetization and suitable magnetic properties [50–53]. In addition, recent efforts on various composites with magnetic particles with different morphologies have been made to improve the stability of MR suspensions. Among these magnetic particles, soft-magnetic CI microspheres are commonly used as an MR dispersed phase but the large density mismatch between the pure CI particles and dispersing medium oil generates serious sedimentation problems. Therefore, to overcome this drawback, a range of additives, including surfactants, organic materials, polymers [54] and different inorganic particles, such as organoclay, CI nanoparticles (NPs), fumed silica, carbon nanotubes (CNTs), carbon fibers, and graphene oxide (GO), have been introduced. Furthermore, in addition to additive systems, coating technology on the surface of CI particles has also been introduced. Inorganic or polymeric materials with low density have been used to coat the surface of CI particles. The expected enhancements in the suspension stability were obtained compared to that of pure CI particle-based MR suspension. In addition, rough CNTs were also introduced on the smooth surface of polymer- or silica-coated CI particles using a dual-step coating technology to enhance the interaction of the adjacent particles and avoid the settling problem. The detailed contents will be discussed in the following section.

3. Morphology

Recently, graphene, a monolayer of carbon atoms, or GO-based materials have been studied widely because of their interesting properties. In particular, the GO sheet can be regarded as an ideal precursor material for graphene, bearing oxygen functional groups on its basal plane and sheet edge, which provides good dispersion stability in aqueous and other common organic solvents. In addition, pure GO sheets or GO-based composites can be developed as novel ER candidates. The electrical conductivity range of GO sheets is favorable to ER applications and their intrinsic polar property is expected to improve the interfacial polarization [55]. To date, diverse fabricated strategies toward fabricating graphene/GO-based ER materials with a variety of particle shapes have been developed. A silica-GO hybrid composite produced by the hydrolysis of tetraethyl orthosilicate (TEOS) on GO sheets have been reported, as shown in Figure 1a, in which the silica NPs were anchored to the GO layers [56]. Furthermore, conducting PANI has been studied extensively as one of the most important

ER materials because of its simple preparation, good thermal/environmental stability and controllable electrical conductivity. Yin *et al*. [57] introduced PANI-coated graphene sheets that exhibit an enhanced ER effect compared to that of a traditional PANI granule suspension under an electric field.

On the other hand, compared to the irregular composites, particles with a narrow particle size distribution are needed to provide more appealing properties. Dong *et al.* [58] reported novel hydrophobic poly[2-(methacryloyloxy)ethyl-trimethylammonium bis(trifluoromethane sulfonyl)imide] (P[MTMA][TFSI]) microspheres by microwave-assisted dispersion polymerization, in which the low particle density and ionic parts provide a P[MTMA][TFSI] microsphere-based ER system good dispersion stability and high ER effect.

Compared to various ER materials with irregular shapes, core-shell structured particles are considered a type of ideal design structure for ER materials, where the particle size and shape, ER activity, particle density, and electrical conductivity can be well controlled. As shown in Figure 1d–f, different core-shell structured GO/polystyrene (PS), silica/polythiophene (PT), poly(glycidyl methacrylate) (PGMA)/PANI particles were reported with the expected ER properties [59–61].

Nonetheless, compared to spherical particles, particles with an elongated or anisotropic shape were expected to have enhanced field-induced dipole moments [62]. The fibrous PANI-based ER fluid showed an improved ER effect [63]. Liu *et al*. [64] reported that silica NPs modified PANI nanofiber (PANIF)-based ER systems exhibited a higher ER effect than that of the pure PANIF.

Figure 1. SEM (scanning electron microscope) images of (**a**) silica- graphene oxide (GO) composite (Reprinted with permission from [56], copyright 2008 American Chemical Society); (**b**) PANI decorated graphene sheets (Reprinted with permission from [57], copyright 2012 Royal Society of Chemistry); (**c**) P[MTMA][TFSI] microspheres (Reprinted with permission from [58], copyright 2014 Royal Society of Chemistry); (**d**) core-shell structured GO coated polystyrene (PS) (Reprinted with permission from [59], copyright 2011 Royal Society of Chemistry); (**e**) silica/polythiophene (PT) nanospheres (Reprinted with permission from [60], copyright 2009 Royal Society of Chemistry); (**f**) PGMA (poly(glycidyl methacrylate))/PANI particles (Reprinted with permission from [61], copyright 2013 Elsevier); (**g**) fibrous PANI particles (Reprinted with permission from [63], copyright 2008 Elsevier); and (**h**) silica nanoparticle modified PANI nanofibers (Reprinted with permission from [64], copyright 2011 Royal Society of Chemistry).

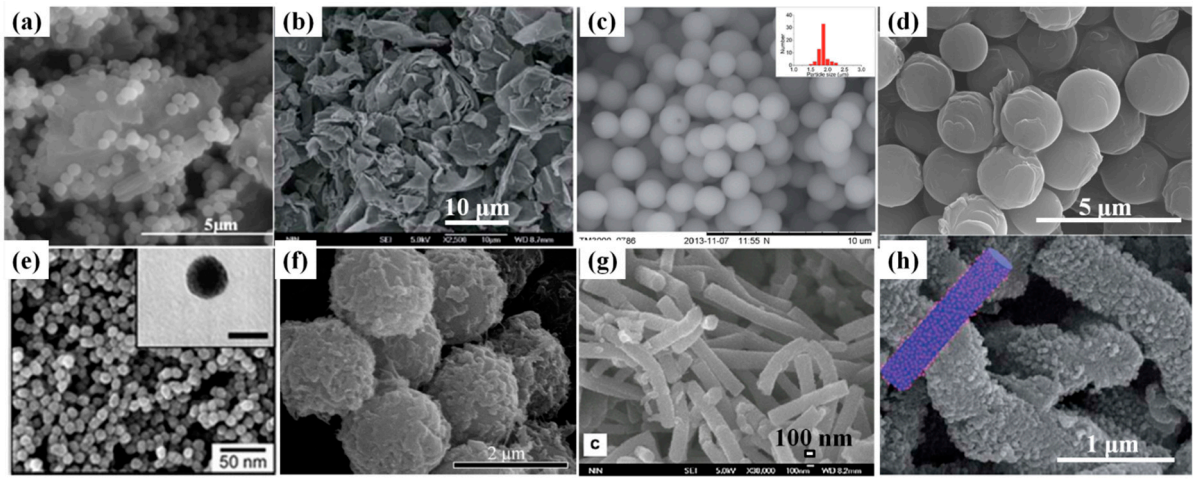

In addition, materials derived from a host-guest interaction were also reported to be interesting ER candidates with an enhanced ER effect. Geist *et al*. [65] reported the eco-friendly intercalation of metallosupramolecular polyelectrolytes into layered silicate via electrostatic interactions and showed their concentration-dependent ER performance. ER fluids based on particles composed of conducting PPy or rigid-rod-like MEPEs intercalated in mesoporous silicate (SBA-15) exhibit a notable ER effect [66,67]. The inner channels of mesoporous silica (MCM-41) were also modified by high polarizable materials, such as PANI, PPy or triethanolamine, and showed enhanced ER behaviors [68–71].

Concurrently, in the case of magneto-responsive particles, soft-magnetic CI microspheres are typical magnetizable particles for MR suspensions because of their excellent magnetic properties, high saturation magnetization and almost zero magnetic hysteresis. To decrease the density mismatch of CI particles and dispersing medium, multi-walled CNTs (MWCNTs) or GO sheets were coated onto the surface of CI particles, adopting a grafting agent, 4-aminobenzoic acid (PABA). As shown in Figure 2a,b, compared to the smooth surface of pure CI, the surface of modified CI particles using GO become considerably rough. The modification of CI particles using polymer coating technology becomes increasingly predominant because of the favorable morphology, good stability in oils and obvious decrease in density [72]. Therefore, considerable effort has been made to coat CI with a range of polymers, such as PS, PANI and polycarbonate (PC) [73–75]. The smooth surface of polymer-coated CI particles itself might not have a positive effect on improving the settling problem in terms of friction. The PS nanobeads were first deposited on the surface of CI particles through conventional dispersion polymerization. Subsequently, dense MWCNT nests were constructed over the surface of the PS-coated CI particles self-assembly using a simple solvent-casting method. Similarly, PANI-coated CI particles were coated with MWCNT to enhance the surface roughness [76].

Figure 2. SEM images of (**a**) pure CI (Reprinted with permission from [72], copyright 2014 AIP Publishing); (**b**) GO coated CI particles (Reprinted with permission from [72]); (**c**) PS coated carbonyl iron (CI) (Reprinted with permission from [73], copyright 2010 American Chemical Society); (**d**) MWCNT wrapped PS/CI magnetic particles (Reprinted with permission from [73]); (**e**) PS/Fe_2O_3 particles (Reprinted with permission from [52], copyright 2013 American Chemical Society); (**f**) Fe_3O_4 coated microporous PS particles (Reprinted with permission from [77], copyright 2009 Elsevier); (**g**) CNT/Fe_3O_4 nanocomposites and CNTs (Reprinted with permission from [53], copyright 2005 Wiley); and (**h**) Fe_3O_4/PMMA (Reprinted with permission from [78], copyright 2008 Elsevier).

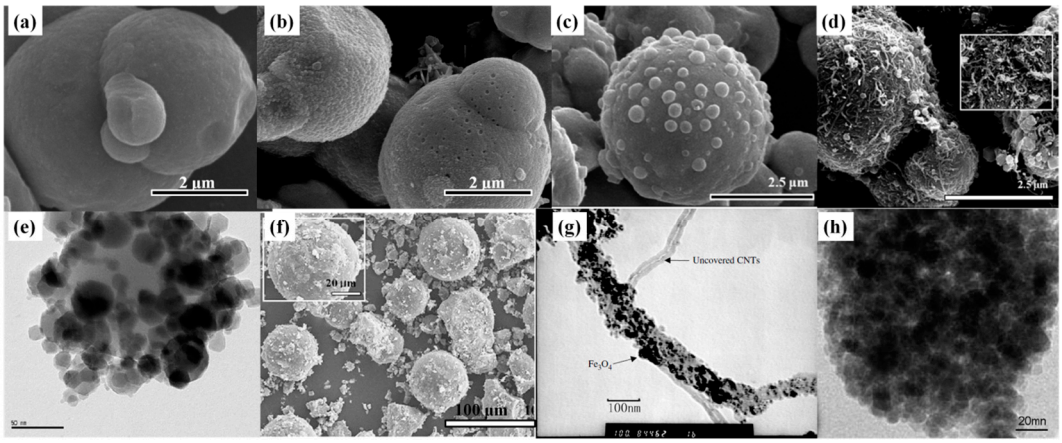

In particular, Fe_2O_3 NPs have attracted considerable interest for MR applications with a lower density than CI particles and significant magnetic behavior. Kim *et al*. [52] reported core-shell structured PS/Fe_2O_3 particles constructed by the Pickering emulsion process. The Pickering emulsion technique is considered an eco-friendly strategy, where the solid inorganic particles are used as a stabilizer instead of conventional organic surfactants. The incorporation of a PS core can reduce the density of the magnetic particles and improve the dispersibility of Fe_2O_3 NPs. Another magnetic species, Fe_3O_4 particles, have also been introduced as MR candidates. To reduce the particle density and improve the magnetic property, Fang *et al*. reported Fe_3O_4-coated microporous PS particles [77].

Various Fe_3O_4-based composites with inorganic or organic components have been reported to be excellent MR candidates with enhanced dispersion stability. CNT/Fe_3O_4 nanocomposites have been reported [53], and Fe_3O_4/PMMA composite particles were fabricated successfully using a simple one-pot hydrothermal method [78], shown in Figure 2g,h, respectively. Detailed experimental and theoretical research about the MR characteristics of fiber suspensions have been reported, and the fiber suspensions have a positive effect on the MR performance but its influence on the yield stress is not significant [79,80].

The particle geometry is known to be a critical factor which is directly related to the ER activity, and Lee *et al*. [81] have studied the ER performances of GO-wrapped silica particles with different aspect ratio. As shown in Figure 3, the higher dynamic yield stress was obtained with increasing aspect ratio of the dispersed particles, in which the high aspect ratio increases the dynamic drag force, resulting in a high flow resistance inducing high shear stress. In addition, the particles with high aspect ratio exhibits strong mechanical stability during the formation of fibril-structure under external electric field strength, therefore demonstrates high shear stress [81].

Figure 3. The comparison of dynamic yield stress of GO-wrapped silica particles based ER fluids with different aspect ratio (Reprinted with permission from [81], copyright 2014 Royal Society of Chemistry).

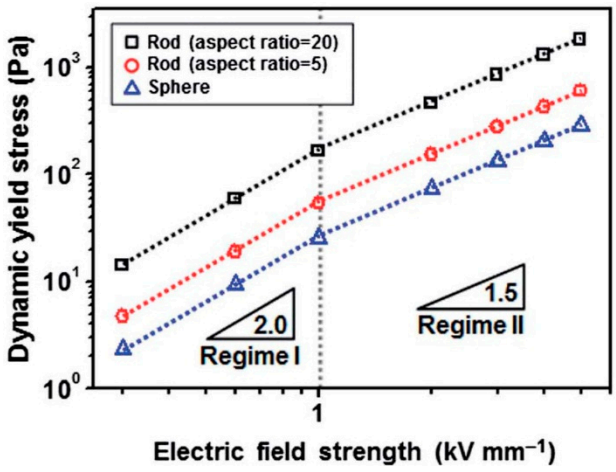

4. Typical Characteristics and Rheological Analysis

As mentioned above, mesoporous materials are interesting ER materials. Different materials with high polarizability can be introduced in the channels of these mesoporous particles, such as SBA-15 and MCM-41, to improve their ER effects. The pore volume can be calculated from the nitrogen

adsorption-desorption isotherms, which provide reliable evidence for the existence of particles in the channels of the mesoporous hosts. As shown in Figure 4, after the formation of PPy and PANI particles inside the channels of these mesoporous silica hosts [67,71], the residual pore volumes of PPy-SBA-15 and PANI/MCM-41 decrease compared to those of the pure mesoporous SBA-15 or MCM-41 silica hosts, confirming the presence of these conducting polymers inside the channels.

Figure 4. Comparison of the nitrogen adsorption-desorption isotherms of (**a**) SBA-15 and PPy-SBA-15 (Reprinted with permission from [67], copyright 2006 Elsevier); and (**b**) pristine MCM-41 and PANI/MCM-41 (Reprinted with permission from [71], copyright 2004 American Chemical Society).

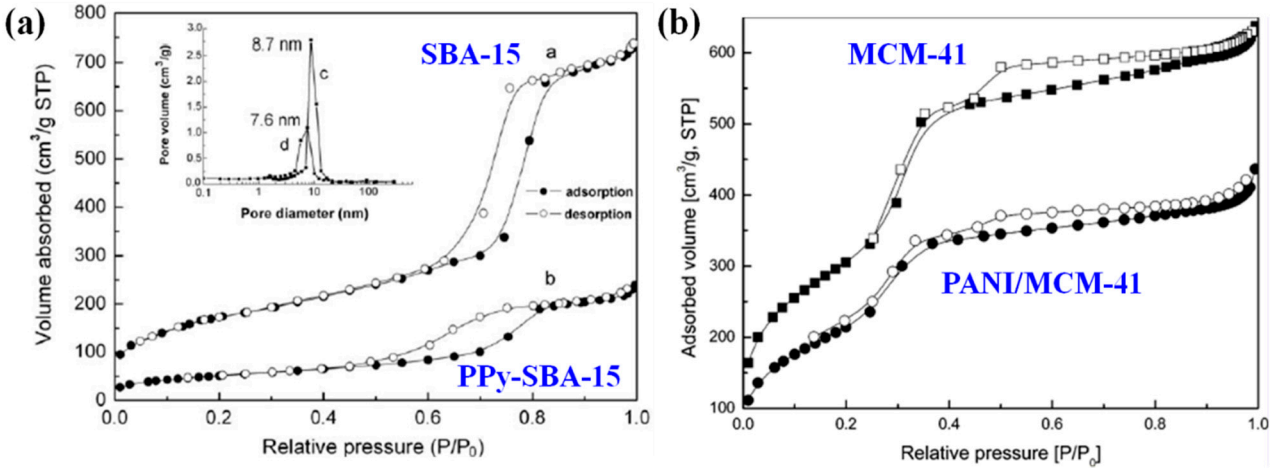

Optical microscopy (OM) imaging is a facile way of observing the formed chain-structure visible for ER or MR materials under an external electric or magnetic field, respectively. As shown in Figure 5, the free-flow GO sheet-based ER suspension formed a chain-like structure when exposed to an applied electric field. The fibrous chain-like structures became much denser at a longer time (99.9 ms) [82].

Figure 5. (**a**–**d**) Optical microscopy images of GO suspension (5 wt%, particle concentration in silicone oil) under an external electric field (1 kV·mm^{-1}) ((Reprinted with permission from [82], copyright 2012 Royal Society of Chemistry).

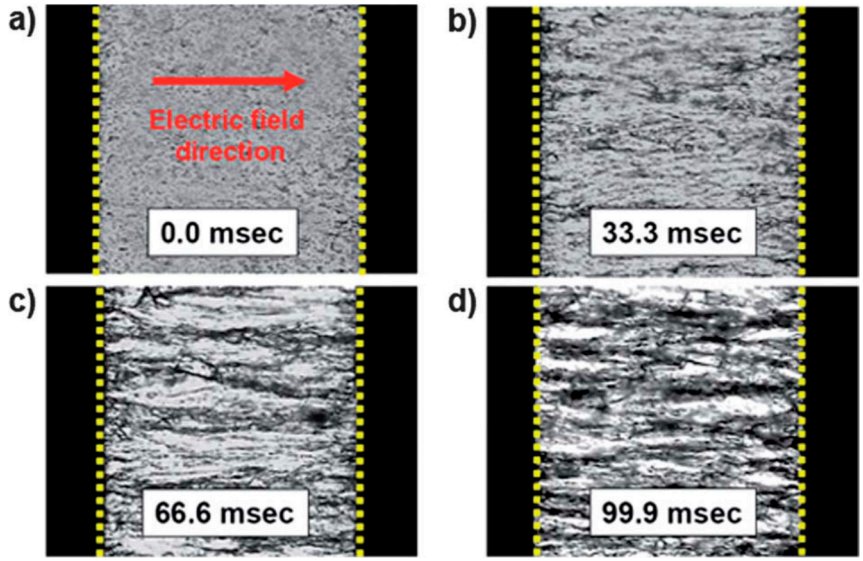

Figure 6 shows the flow curves of the shear stress as a function of the shear rate for Si–GO composite-based ER fluids measured using a rotational rheometer in a controlled shear rate (CSR) mode. The dispersed particles were polarized and formed field-induced fibrous structures. These formed fibrous structure become robust, resulting in enhanced shear stress with increasing electric field strength. A traditional Bingham equation and Cho–Choi–Jhon (CCJ) model with six parameters were applied to analyze the flow curves. As a general model for an ER fluid, the Bingham fluid model is described as:

$$\begin{aligned} \tau &= \tau_0 + \eta_0 \dot{\gamma}, \qquad \tau \geq \tau_0 \\ \dot{\gamma} &= 0, \qquad \tau < \tau_0 \end{aligned} \tag{1}$$

where τ is the shear stress, τ_0 is the yield stress, η_0 is the shear viscosity, and $\dot{\gamma}$ is the shear rate. The simple Bingham fluid model cannot cover the shear stress curves well. A suggested model called the Cho–Choi–Jhon (CCJ) model [83] with six parameters has been adopted:

$$\tau = \frac{\tau_0}{1+(t_1\dot{\gamma})^{\alpha}} + \eta_{\infty}\left(1+\frac{1}{(t_2\dot{\gamma})^{\beta}}\right)\dot{\gamma} \tag{2}$$

Here, τ_0 is the dynamic yield stress; η_∞ is the shear viscosity at infinite shear rate and also is considered as the shear viscosity in the absence of electric field; t_1 and t_2 are time constants used to describe the variation in shear stress; the exponent α is related to the decrease of shear stress at low shear rate region, while β in the range of 0–1 is for the high shear rate region. The two terms in the right-hand side of the equation can represent the shear stress in different shear rate regions. The first term in the equation implies the shear stress behavior at a low shear rate region especially in the case of the decrease of shear rate. In addition, the second one controls the fitting in a high shear rate region where the shear stress increases and then tends to converge to a uniform line as the shear rate reaches to an extremely high value. The exponent β has the range $0 < \beta \leq 1$, because $d\tau / d\dot{\gamma} \geq 0$ [84]. Note that the CCJ model has been also adopted into various ER materials [85,86].

Figure 6. Shear stress *vs.* shear rate for a Si–GO composite-based ER fluid. The solid and dotted lines are fitted to the Cho–Choi–Jhon (CCJ) and Bingham models, respectively (Reprinted with permission from [33], copyright 2014 SPIE).

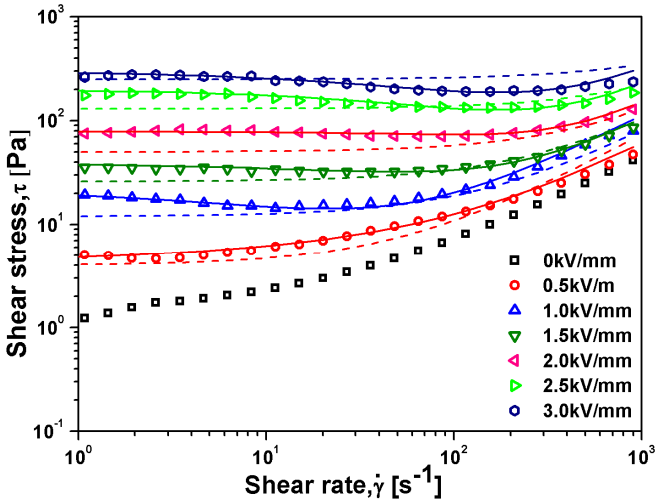

Furthermore, the physical meanings of the flow curve given in Figure 6 along with the CCJ model can be explained based on the mechanism that the fibrillation of ER particles in the shear flow is a breaking and re-formation process caused by the cooperation of electrostatic attractive and hydrodynamic repulsive interactions, which are reduced by an external electric and flow field. In the low shear rate region, where the electrostatic interaction is dominant, the aligned particles begin to break with shear deformation and the broken structures tend to re-form chains again. However, the rate of destruction may be faster than the rate of re-formation. Therefore, the shear stress generated decreases with increasing shear rate. Hydrodynamic repulsive interactions dominate in the high shear rate region, where fibril particle structures are fully destroyed without re-formation, and the suspension behaves like a pseudo-Newtonian fluid [84]. Compared to the Bingham model, the suggested CCJ model explained the experimental flow curves well, particularly at the low shear rate range.

Similar to an ER fluid, the dynamic yield stress τ_y for a MWCNT/PANI/CI-based MR fluid was obtained from the shear stress curves and replotted as a function of the magnetic field strength H, as shown in Figure 7a. At a weak range of H, the relationship between τ_y and H can be described as $\tau_y \propto H^2$. With increasing H, the local saturation becomes prominent, and τ_y can be expressed as follows:

$$\tau_y = \sqrt{6}\phi\mu_0 M_s^{1/2} H^{3/2} \tag{3}$$

where M_s is the saturation magnetization, μ_0 is the permeability of free space and ϕ is the volume fraction of the particles. The magnetic particles reach saturation at a critical magnetic field strength, where τ_y is not dependent on H:

$$\tau_y^{sat} = 0.086\phi\mu_0 M_s^2 \tag{4}$$

As shown in Figure 7a, there is a critical H_c, where τ_y increases quadratically with increasing H_0 ($H_0 << H_c$), and the slope of τ_y *vs*. H then turns to 1.5 ($H_0 >> H_c$). The relationship can be displayed as a new universal equation using this critical H_c:

$$\tau_y(H_0) = \alpha H_0^2 \left(\frac{\tan\sqrt{H_0/H_c}}{\sqrt{H_0/H_c}}\right) \tag{5}$$

$$\begin{aligned} \tau_y &= \alpha H_0^2 \quad \text{for } H_0 << H_c \\ \tau_y &= \alpha\sqrt{H_c} H_0^{3/2} \quad \text{for } H_0 >> H_c \end{aligned} \tag{6}$$

In addition, similar to an ER fluid, a generalized relationship can be obtained using H_c and $\tau_y(H_c) = 0.762\alpha H_c^2$ to study MR fluids:

$$\hat{\tau} = 1.313\widehat{H}^{3/2} \tanh\sqrt{\widehat{H}} \tag{7}$$

The data obtained from Figure 7a was collapsed onto a single line using the generalized relationship shown in Figure 7b.

Figure 7. (**a**) Dynamic yield stress *vs.* magnetic field strength and (**b**) $\hat{\tau}$ *vs.* $\hat{H}$ for MWCNT/PANI/CI-based MR suspension (Reprinted with permission from [76], copyright 2004 American Chemical Society).

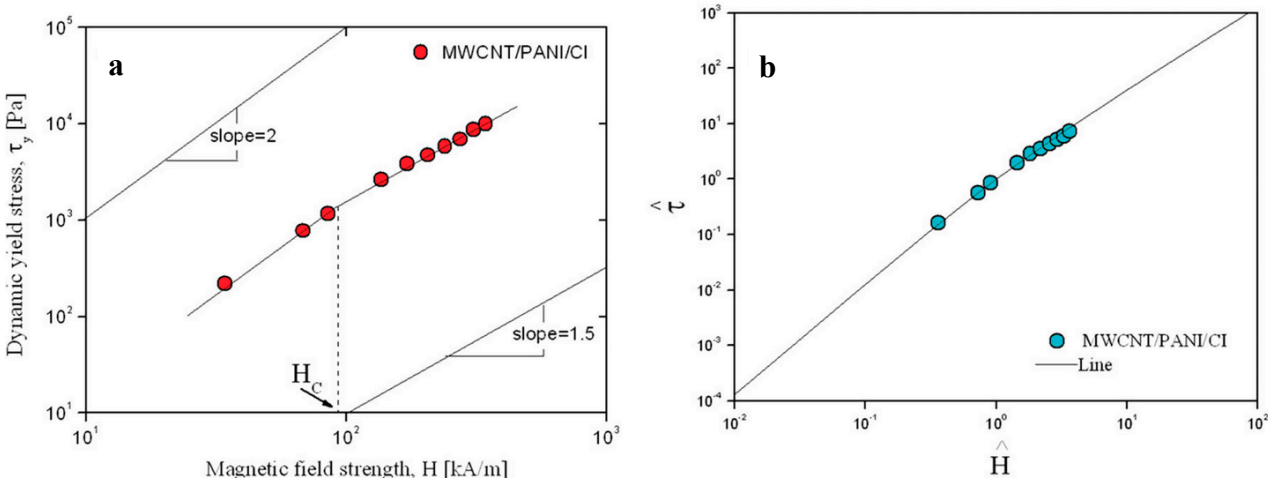

A creep and recovery test can be carried out to examine the deformation of the particle structures under an electric field with or without a loading. Liu *et al*. [87] reported the creep and recovery test of poly(styrene-*co*-butylacrylate-*co*-[2-(methacryloxy)ethyl]trimethylammonium chloride)/(PSBM)/SiO_2-based ER fluids. As shown in Figure 8, once the shear stress is applied, instantaneous strain appears and increases as a function of time until it approaches a maximum. The ER fluid becomes more solid-like (*i.e.*, $\gamma_{max,2} << \gamma_{max,1}$) under a higher electric field strength [88].

Figure 8. Creep and recovery test for PSBM/SiO_2 based ER fluid (Reprinted with permission from [87], copyright 2014 American Chemical Society).

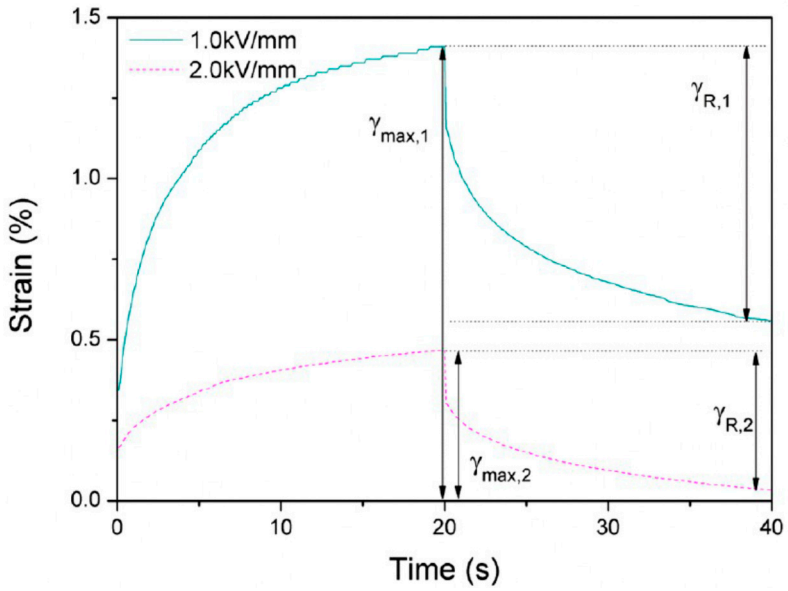

5. Conclusions

Inorganic colloidal or polymeric composite materials with a well-designed morphology have been applied as good candidates for electro-responsive ER materials with enhanced ER activity and good

suspension stability. Graphene/GO-based composites exhibited an appealing ER effect, and core-shell structured particles composed of highly polarizable core or shell materials were included. The elongated morphology played a positive role in enhancing the ER effect. Regarding magneto-responsive MR particles, GO or MWCNT coated on the surface of CI particles can decrease the particle density and improve the suspension stability. A coating of MWCNTs after polymer-coated CI particle was reported to enhance the interaction of the particles. In addition, many iron oxide composites have been fabricated and reported to be MR candidates using a variety of strategies, particularly the eco-friendly Pickering polymerization method. Overall, this paper briefly reviewed the characteristics of ER and MR fluids.

Acknowledgments

This study was supported by Ministry of Trade, Industry and Energy, Korea through Daeheung RNT (# 10047791).

Conflicts of Interest

The authors declare no conflict of interest.

References

1. Dai, S.; Ravi, P.; Tam, K.C. Thermo- and photo-responsive polymeric systems. *Soft Matter* **2009**, *5*, 2513–2533.
2. Wu, X.; Huang, W.M.; Zhao, Y.; Ding, Z.; Tang, C.; Zhang, J. Mechanisms of the shape memory effect in polymeric materials. *Polymers* **2013**, *5*, 1169–1202.
3. Choi, H.J.; Lee, Y.H.; Kim, C.A.; Jhon, M.S. Microencapsulated polyaniline particles for electrorheological materials. *J. Mater. Sci. Lett.* **2000**, *19*, 533–535.
4. Aucoin, H.R.; Wilson, A.N.; Wilson, A.M.; Ishihara, K.; Guiseppi-Elie, A. Release of potassium ion and calcium ion from phosphorylcholine group bearing hydrogels. *Polymers* **2013**, *5*, 1241–1257.
5. Wu, J.; Jin, T.; Liu, E.; Guo, J.; Cheng, Y.; Xu, G. Formamide-modified titanium oxide nanoparticles with high electrorheological activity. *RSC Adv.* **2014**, *4*, 29622–29628.
6. Parthasarathy, M.; Klingenberg, D.J. Electrorheology: Mechanisms and models. *Mater. Sci. Eng. R* **1996**, *17*, 57–103.
7. Choi, H.J.; Jhon, M.S. Electrorheology of polymers and nanocomposites. *Soft Matter* **2009**, *5*, 1562–1567.
8. Marins, J.A.; Dahmouche, K.; Soares, B.G. New electrorheological fluid obtained from mercaptosilsesquioxane-modified silicate suspensions. *Mater. Sci. Eng. C* **2013**, *33*, 133–139.
9. Li, C.L.; Chen, J.K.; Fan, S.K.; Ko, F.H.; Chang, F.C. Electrorheological operation of low-/high-permittivity core/shell sio2/au nanoparticle microspheres for display media. *ACS Appl. Mater. Interface* **2012**, *4*, 5650–5661.
10. Kontopoulou, M.; Kaufman, M.; Docoslis, A. Electrorheological properties of PDMS/carbon black suspensions under shear flow. *Rheol. Acta* **2009**, *48*, 409–421.

11. Song, X.; Song, K.; Ding, S.; Chen, Y.; Lin, Y. Electrorheological properties of poly[*N*,*N*'-(2-amino-5-carboxybutyl-1,3-phenylenedimethylene)-2,2'-diamino-4,4'-bithiazole]. *J. Ind. Eng. Chem.* **2013**, *19*, 416–420.
12. Hiamtup, P.; Sirivat, A.; Jamieson, A.M. Hysteresis and strain hardening in the creep response of a polyaniline ER fluid. *J. Colloid Interface Sci.* **2008**, *325*, 122–129.
13. Yilmaz, H.; Zengin, H.; Unal, H.I. Synthesis and electrorheological properties of polyaniline/silicon dioxide composites. *J. Mater. Sci.* **2012**, *47*, 5276–5286.
14. Orihara, H.; Nishimoto, Y.; Aida, K.; Na, Y.H. Three-dimensional observation of an immiscible polymer blend subjected to a step electric field under shear flow. *Phys. Rev. E* **2011**, *83*, doi:10.1103/PhysRevE.83.026302.
15. Rodrıguez-Arco, L.; Lopez-Lopez, M.T.; Kuzhir, P.; Duran, J.D.G. Steady state rheological behaviour of multi-component magnetic suspensions. *Soft Matter* **2013**, *9*, 5726–5737.
16. Chen, K.; Tian, Y.; Shan, L.; Zhang, X.; Meng, Y. The rheological properties of magnetic field excited magnetic powders sheared between two parallel plates. *Smart Mater. Struct.* **2013**, *22*, doi:10.1088/0964-1726/22/11/115036.
17. Seo, Y.P.; Seo, Y. Modeling and analysis of electrorheological suspensions in shear flow. *Langmuir* **2012**, *28*, 3077–3084.
18. Kim, Y.D.; Kim, H.S. Negative electrorheological responses of mono-dispersed polypyrrole-san copolymer suspensions. *Macromol. Res.* **2013**, *21*, 1153–1158.
19. Schwarz, G.; Haßlauer, I.; Kurth, D.G. From terpyridine-based assemblies to metallo-supramolecular polyelectrolytes (MEPEs). *Adv. Colloid Interface Sci.* **2014**, *207*, 107–120.
20. Cheng, Q.; Pavlinek, V.; He, Y.; Yan, Y.; Li, C.; Saha, P. Synthesis and electrorheological characteristics of sea urchin-like TiO_2 hollow spheres. *Colloid Polym. Sci.* **2011**, *289*, 799–805.
21. Seo, Y. A new yield stress scaling function for electrorheological fluids. *J. Non-Newton. Fluid Mech.* **2011**, *166*, 241–243.
22. Ginder, J.M.; Davis, L.C.; Elie, L.D. Rheology of magnetorheological fluids: Models and measurements. *Int. J. Mod. Phys. B* **1996**, *10*, 3293–3303.
23. De Vicente, J.; Klingenberg, D.J.; Hidalgo-Alvarez, R. Magnetorheological fluids: A review. *Soft Matter* **2011**, *7*, 3701–3710.
24. Guerrero-Sanchez, C.; Lara-Ceniceros, T.; Jimenez-Legalado, E.; Rasa, M.; Schubert, U.S. Magnetorheological fluids based on ionic liquids. *Adv. Mater.* **2007**, *19*, 1740–1747.
25. Bossis, G.; Lacis, S.; Meunier, A.; Volkova, O. Magnetorheological fluids. *J. Magn. Magn. Mater.* **2002**, *252*, 224–228.
26. Tang, X.; Zhang, X.; Tao, R.; Rong, Y.M. Structure-enhanced yield stress of magnetorheological fluids. *J. Appl. Phys.* **2000**, *87*, 2634–2638.
27. Wen, W.J.; Huang, X.X.; Sheng, P. Electrorheological fluids: Structures and mechanisms. *Soft Matter* **2008**, *4*, 200–210.
28. Qian, B.; McKinley, G.H.; Hosoi, A.E. Structure evolution in electrorheological fluids flowing through microchannels. *Soft Matter* **2013**, *9*, 2889–2898.
29. Tao, R.; Du, E.; Tang, H.; Xu, X. Neutron scattering studies of crude oil viscosity reduction with electric field. *Fuel* **2014**, *134*, 493–498.

30. Goncalves, J.L.; Bombard, A.J.F.; Soares, D.A.W.; Alcantara, G.B. Reduction of paraffin precipitation and viscosity of brazilian crude oil exposed to magnetic fields. *Energy Fuels* **2010**, *24*, 3144–3149.
31. Bica, I. Damper with magnetorheological suspension. *J. Magn. Magn. Mater.* **2002**, *241*, 196–200.
32. Kemmetmuller, W.; Holzmann, K.; Kugi, A.; Stork, M. Electrorheological semiactive shock isolation platform for naval applications. *IEEE-ASME Trans. Mechatron.* **2013**, *18*, 1437–1447.
33. Sidpara, A. Magnetorheological finishing: A perfect solution to nanofinishing requirements. *Opt. Eng.* **2014**, *53*, doi:10.1117/1.OE.53.9.092002.
34. Seong, M.S.; Choi, S.B.; Kim, C.H. Design and performance evaluation of MR damper for integrated Isolation mount. *J. Intel. Mater. Sys. Struct.* **2011**, *22*, 1729–1738.
35. Rossa, C.; Eck, L.; Micaelli, A.; Lozada, J. On a novel torque detection technique for magnetorheological actuators. *IEEE Sens. J.* **2014**, *14*, 1223–1231.
36. Wang, B.X.; Zhao, Y.; Zhao, X.P. The wettability, size effect and electrorheological activity of modified titanium oxide nanoparticles. *Colloids Surf. A Physicochem. Eng. Asp.* **2007**, *295*, 27–33.
37. See, H.; Kawai, A.; Ikazaki, F. The effect of mixing particles of different size on the electrorheological response under steady shear flow. *Rheol. Acta* **2002**, *41*, 55–60.
38. Lengalova, A.; Pavlinek, V.; Saha, P.; Quadrat, O.; Kitano, T.; Steiskal, J. Influence of particle concentration on the electrorheological efficiency of polyaniline suspensions. *Eur. Polym. J.* **2003**, *39*, 641–645.
39. El Wahed, A.K. The influence of solid-phase concentration on the performance of electrorheological fluids in dynamic squeeze flow. *Mater. Des.* **2011**, *32*, 1420–1426.
40. Yin, J.B.; Zhao, X.P. Preparation and electrorheological activity of mesoporous rare-earth-doped TiO_2. *Chem. Mater.* **2002**, *14*, 4633–4640.
41. Yin, J.B.; Shui, Y.J.; Chang, R.T.; Zhao, X.P. Graphene-supported carbonaceous dielectric sheets and their electrorheology. *Carbon* **2012**, *50*, 5247–5255.
42. Cheng, Y.C.; Guo, J.J.; Liu, X.H.; Sun, A.H.; Xu, G.J.; Cui, P. Preparation of uniform titania microspheres with good electrorheological performance and their size effect. *J. Mater. Chem.* **2011**, *21*, 5051–5056.
43. Tian, Y.; Meng, Y.G.; Wen, S.Z. Electrorheology of a zeolite/silicone oil suspension under DC fields. *J. Appl. Phys.* **2001**, *90*, 493–496.
44. Clercx, H.J.H.; Bossis, G. Many-body electrostatic interactions in electrorheological fluids. *Phys. Rev. E* **1993**, *48*, 2721–2738.
45. Martin, J.E.; Anderson, R.A.; Williamson, R.L. Generating strange interactions in particle suspensions. *Compos. Sci. Technol.* **2003**, *63*, 1097–1103.
46. Anderson, R.A.; Martin, J.E. Energy balance problems in systems of induced and permanent electric and magnetic dipoles. *Am. J. Phys.* **2002**, *70*, 1194–1204.
47. Martin, J.E.; Anderson, R.A. Chain model of electrorheology. *J. Chem. Phys.* **1996**, *104*, 4814–4827.
48. Martin, J.E.; Odinek, J.; Halsey, T.C.; Kamien, R. Structure and dynamics of electrorheological fluids. *Phys. Rev. E* **1998**, *57*, 756–775.
49. Espin, M.J.; Delgado, A.V.; Martin, J.E. Effects of electric fields and volume fraction on the rheology of hematite/silicone oil suspensions. *Rheol. Acta* **2004**, *44*, 71–79.

50. Cho, M.S.; Lim, S.T.; Jang, I.B.; Choi, H.J.; Jhon, M.S. Encapsulation of spherical iron-particle with PMMA and its magnetorheological particles. *IEEE Trans. Magn.* **2004**, *40*, 3036–3038.
51. Margida, A.J.; Weiss, K.D.; Carlson, J.D. Magnetorheological materials based on iron alloy particles. *Int. J. Mod. Phys. B* **1996**, *10*, 3335–3341.
52. Kim, Y.J.; Liu, Y.D.; Seo, Y.; Choi, H.J. Pickering-emulsion-polymerized polystyrene/Fe_2O_3 composite particles and their magnetoresponsive characteristics. *Langmuir* **2013**, *29*, 4959–4965.
53. Pu, H.T.; Jiang, F.J. Towards high sedimentation stability: Magnetorheological fluids based on CNT/Fe_3O_4 nanocomposites. *Nanotechnology* **2005**, *16*, 1486–1489.
54. Lopez-Lopez, M.T.; Gomez-Ramirez, A.; Duran, J.D.G.; Gonzalez-Caballero, F. Preparation and characterization of iron-based magnetorheological fluids stabilized by addition of organoclay particles. *Langmuir* **2008**, *24*, 7076–7084.
55. Yin, J.; Shui, Y.; Dong, Y.; Zhao, X. Enhanced dielectric polarization and electro-responsive characteristic of graphene oxide-wrapped titania microspheres. *Nanotechnology* **2014**, *25*, doi:10.1088/0957-4484/25/4/045702.
56. Zhang, W.L.; Choi, H.J. Silica-graphene oxide hybrid composite particles and their electroresponsive characteristics. *Langmuir* **2012**, *28*, 7055–7062.
57. Yin, J.B.; Wang, X.X.; Chang, R.T.; Zhao, X.P. Polyaniline decorated graphene sheet suspension with enhanced electrorheology. *Soft Matter* **2012**, *8*, 294–297.
58. Dong, Y.Z.; Yin, J.B.; Zhao, X.P. Microwave-synthesized poly(ionic liquid) particles: A new material with high electrorheological activity. *J. Mater. Chem. A* **2014**, *2*, 9812–9819.
59. Zhang, W.L.; Liu, Y.D.; Choi, H.J. Graphene oxide coated core-shell structured polystyrene microspheres and their electrorheological characteristics under applied electric field. *J. Mater. Chem.* **2011**, *21*, 6916–6921.
60. Hong, J.Y.; Kwon, E.; Jang, J. Fabrication of silica/polythiophene core/shell nanospheres and their electrorheological fluid application. *Soft Matter* **2009**, *5*, 951–953.
61. Zhang, W.L.; Piao, S.H.; Choi, H.J. Facile and fast synthesis of polyaniline-coated poly(glycidyl methacrylate) core-shell microspheres and their electro-responsive characteristics. *J. Colloid Interface Sci.* **2013**, *402*, 100–106.
62. Tsuda, K.; Takeda, Y.; Ogura, H.; Otsubo, Y. Electrorheological behavior of whisker suspensions under oscillatory shear. *Colloids Surf. A Physicochem. Eng. Asp.* **2007**, *299*, 262–267.
63. Yin, J.B.; Zhao, X.P.; Xia, X.; Xiang, L.Q.; Qiao, Y.P. Electrorheological fluids based on nano-fibrous polyaniline. *Polymer* **2008**, *49*, 4413–4419.
64. Liu, Y.D.; Fang, F.F.; Choi, H.J. Silica nanoparticle decorated polyaniline nanofiber and its electrorheological response. *Soft Matter* **2011**, *7*, 2782–2789.
65. Geist, M.F.; Boussois, K.; Smith, A.; Peyratout, C.S.; Kurth, D.G. Nanocomposites derived from montmorillonite and metallosupramolecular polyelectrolytes: Modular compounds for electrorheological fluids. *Langmuir* **2013**, *29*, 1743–1747.
66. Schwarz, G.; Maisch, S.; Ullrich, S.; Wagenhofer, J.; Kurth, D.G. Electrorheological fluids based on metallo-supramolecular polyelectrolyte-silicate composites. *ACS Appl. Mater. Interfaces* **2013**, *5*, 4031–4034.

67. Cheng, Q.L.; Pavlinek, V.; Lengalova, A.; Li, C.Z.; He, Y.; Saha, P. Conducting polypyrrole confined in ordered mesoporous silica SBA-15 channels: Preparation and its electrorheology. *Microporous Mesoporous Mater.* **2006**, *93*, 263–269.
68. Cheng, Q.L.; Pavlinek, V.; He, Y.; Lengalova, A.; Li, C.Z.; Saha, P. Structural and electrorheological properties of mesoporous silica modified with triethanolamine. *Colloids Surf. A Physicochem. Eng. Asp.* **2008**, *318*, 169–174.
69. Cheng, Q.L.; Pavlinek, V.; Lengalova, A.; Li, C.Z.; Belza, T.; Saha, P. Electrorheological properties of new mesoporous material with conducting polypyrrole in mesoporous silica. *Microporous Mesoporous Mater.* **2006**, *94*, 193–199.
70. Cheng, Q.L.; He, Y.; Pavlinek, V.; Lengalova, A.; Li, C.Z.; Saha, P. Preparation and electrorheology of new mesoporous polypyrrole/MCM-41 suspensions. *J. Mater. Sci.* **2006**, *41*, 5047–5049.
71. Cho, M.S.; Choi, H.J.; Ahn, W.S. Enhanced electrorheology of conducting polyaniline confined in MCM-41 channels. *Langmuir* **2004**, *20*, 202–207.
72. Zhang, W.L.; Choi, H.J. Self-assembly of graphene oxide coated soft magnetic carbonyl iron particles and their magnetorheology. *J. Appl. Phys.* **2014**, *115*, doi:10.1063/1.4863381.
73. Fang, F.F.; Choi, H.J.; Seo, Y. Sequential coating of magnetic carbonyliron particles with polystyrene and multiwalled carbon nanotubes and its effect on their magnetorheology. *ACS Appl. Mater. Interfaces* **2010**, *2*, 54–60.
74. Liu, Y.D.; Fang, F.F.; Choi, H.J. Core-shell-structured silica-coated magnetic carbonyl iron microbead and its magnetorheology with anti-acidic characteristics. *Colloid Polym. Sci.* **2011**, *289*, 1295–1298.
75. Fang, F.F.; Liu, Y.D.; Choi, H.J. Fabrication of carbonyl iron embedded polycarbonate composite particles and magnetorheological characterization. *IEEE Trans. Magn.* **2009**, *45*, 2507–2510.
76. Fang, F.F.; Liu, Y.D.; Choi, H.J.; Seo, Y. Core-shell structured carbonyl iron microspheres prepared via dual-step functionality coatings and their magnetorheological response. *ACS Appl. Mater. Interfaces* **2011**, *3*, 3487–3495.
77. Fang, F.F.; Kim, J.H.; Choi, H.J. Synthesis of core-shell structured PS/Fe_3O_4 microbeads and their magnetorheology. *Polymer* **2009**, *50*, 2290–2293.
78. Cao, Z.; Jiang, W.Q.; Ye, X.Z.; Gong, X.L. Preparation of superparamagnetic Fe_3O_4/PMMA nano composites and their magnetorheological characteristics. *J. Magn. Magn. Mater.* **2008**, *320*, 1499–1502.
79. Lopez-Lopez, M.T.; Kuzhir, P.; Bossis, G. Magnetorheology of fiber suspensions. I. Experimental. *J. Rheol.* **2009**, *53*, 115–126.
80. Kuzhir, P.; Lopez-Lopez, M.T.; Bossis, G. Magnetorheology of fiber suspensions. II. Theory. *J. Rheol.* **2009**, *53*, 127–151.
81. Lee, S.; Yoon, C.M.; Hong, J.Y.; Jang, J. Enhanced electrorheological performance of a graphene oxide-wrapped silica rod with a high aspect ratio. *J. Mater. Chem. C* **2014**, *2*, 6010–6016.
82. Hong, J.Y.; Jang, J. Highly stable, concentrated dispersions of graphene oxide sheets and their electro-responsive characteristics. *Soft Matter* **2012**, *8*, 7348–7350.
83. Cho, M.S.; Choi, H.J.; Jhon, M.S. Shear stress analysis of a semiconducting polymer based electrorheological fluid system. *Polymer* **2005**, *46*, 11484–11488.

84. Fang, F.F.; Liu, Y.D.; Lee, I.S.; Choi, H.J. Well controlled core/shell type polymeric microspheres coated with conducting polyaniline: fabrication and electrorheology. *RSC Adv.* **2011**, *1*, 1026–1032.
85. Meheust, Y.; Parmar, K.P.S.; Schjelderupsen, B.; Fossum, J.O. The electrorheology of suspensions of Na-fluorohectorite clay in silicone oil. *J. Rheol.* **2011**, *55*, 809–833.
86. Wang, B.; Rozynek, Z.; Fossum, J.O.; Knudsen, K.; Yu, Y. Guided self-assembly of nanostructured titanium oxide. *Nanotechnology* **2012**, *23*, doi:10.1088/0957-4484/23/7/075706.
87. Liu, Y.D.; Quan, X.; Hwang, B.; Kwon, Y.K.; Choi, H.J. Core-shell-structured monodisperse copolymer/silica particle suspension and its electrorheological response. *Langmuir* **2014**, *30*, 1729–1734.
88. Kim, J.W.; Kim, S.G.; Choi, H.J.; Suh, M.S.; Shin, M.J.; Jhon, M.S. Synthesis and electrorheological characterization of polyaniline and Na^+-Montmorillonite clay nanocomposite. *Int. J. Mod. Phys. B* **2001**, *15*, 657–664.